WL-TR-97-4016

SPLINE VARIATIONAL THEORY FOR COMPOSITE BOLTED JOINTS

E. Iarve

University of Dayton Research Institute
300 College Park Avenue
Dayton, OH 45469-0168

JANUARY 1997

Interim Report for Period 24 January 1996 - 14 September 1996

Approved for public release; distribution unlimited.

MATERIALS DIRECTORATE
WRIGHT LABORATORY
AIR FORCE MATERIEL COMMAND
WRIGHT-PATTERSON AIR FORCE BASE, OH 45433-7734

NOTICE

When government drawings, specifications, or other data are used for any purpose other than in connection with a definitely Government-related procurement, the United States Government incurs no responsibility or any obligation whatsoever. The fact that the government may have formulated or in any way supplied the said drawings, specifications, or other data, is not to be regarded by implication, or otherwise in any manner construed, as licensing the holder, or any other person or corporation; or as conveying any rights or permission to manufacture, use, or sell any patented invention that may be related thereto.

This report is releasable to the National Technical Information Service (NTIS). At NTIS, it will be available to the general public, including foreign nations.

This technical report has been reviewed and is approved for publication.

JAMES R. McCOY, Project Engineer
Structural Materials Branch
Nonmetallic Materials Division

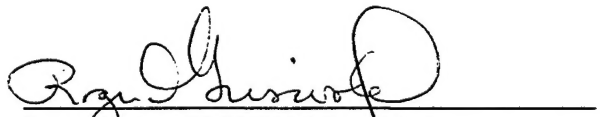

ROGER D. GRISWOLD, Chief
Structural Materials Branch
Nonmetallic Materials Division

L. SCOTT THEIBERT, Assistant Chief
Nonmetallic Materials Division
Materials Directorate

If your address has changed, if you wish to be removed from our mailing list, or if the addressee is no longer employed by your organization, please notify WL/MLBC, Bldg 654, 2941 P St, Ste 1, Wright-Patterson AFB OH 45433-7750 to help us maintain a current mailing list.

Copies of this report should not be returned unless return is required by security considerations, contractual obligations, or notice on a specific document.

REPORT DOCUMENTATION PAGE

Form Approved
OMB No. 0704-0188

1. AGENCY USE ONLY *(Leave blank)*	2. REPORT DATE	3. REPORT TYPE AND DATES COVERED
	JANUARY 1997	Interim - 1/24/96-9/14/96

4. TITLE AND SUBTITLE
SPLINE VARIATIONAL THEORY FOR COMPOSITE BOLTED JOINTS

5. FUNDING NUMBERS
F33615-95-D-5029
PE 62102F
PR 4347
TA 34
WU 10

6. AUTHOR(S)
E. Iarve

7. PERFORMING ORGANIZATION NAME(S) AND ADDRESS(ES)
University of Dayton Research Institute
300 College Park Avenue
Dayton, OH 45469-0168

8. PERFORMING ORGANIZATION REPORT NUMBER
UDR-TR-97-11

9. SPONSORING/MONITORING AGENCY NAME(S) AND ADDRESS(ES)
Materials Directorate
Wright Laboratory
Air Force Materiel Command
Wright-Patterson AFB OH 45433-7734
POC: James R. McCoy, WL/MLBC, 937/255-9063

10. SPONSORING/MONITORING AGENCY REPORT NUMBER
WL-TR-97-4016

11. SUPPLEMENTARY NOTES

12a. DISTRIBUTION/AVAILABILITY STATEMENT
Approved for public release, distribution unlimited.

12b. DISTRIBUTION CODE

13. ABSTRACT *(Maximum 200 words)*

Methods for stress redistribution analysis in composite laminates due to matrix cracking were developed. Two approaches were implemented. A conventional mesh overlay method in the crack region to satisfy the crack face boundary conditions and a novel spline basis partitioning method were compared. The conventional approach failed to provide converged stress continuity boundary conditions at the edge of the overlay mesh. The spline basis partitioning method showed accurate stress boundary conditions at the overlay boundaries and the crack faces. Stress redistribution analysis in [90], [0], and $[0/90]_S$ laminates with matrix cracks emanating from the hole edge has been performed.

14. SUBJECT TERMS composites, damage modeling, finite element, graphite-epoxy, laminates, local field enrichment, matrix cracks, mechanical testing, mechanics modeling, mesh overlay, open-hole spline approximations, splines, SVELT

15. NUMBER OF PAGES 28

16. PRICE CODE

17. SECURITY CLASSIFICATION OF REPORT	18. SECURITY CLASSIFICATION OF THIS PAGE	19. SECURITY CLASSIFICATION OF ABSTRACT	20. LIMITATION OF ABSTRACT
Unclassified	Unclassified	Unclassified	SAR

CONTENTS

FIGURES

FOREWORD

This report was prepared by the University of Dayton Research Institute under Air Force Contract No. F33615-95-D-5029, Delivery Order No. 0004. The work was administered under the direction of the Nonmetallic Materials Division, Materials Directorate, Wright Laboratory, Air Force Materiel Command, with Dr. James R. McCoy (WL/MLBC) as Project Engineer.

This report was submitted in January 1997 and covers work conducted from 24 Jan 1996 through 14 Sep 1996.

1. INTRODUCTION

Development of a damage progression analysis in composites contains an appropriate failure criterion and a numerical algorithm capable of incorporating the formation of new boundaries in the material without restrictions imposed by initial mesh topology. A promising approach to build such a numerical algorithm is local mesh overlay or local field enrichment method described by Mote [1] and more recently by Raju [2], Fish [3], and Reddy [4]. The idea is to add additional degrees of freedom to the initial mesh via superimposing a patch of elements at the location of high local stress gradients, such as those produced by crack tip, etc., which allows one to avoid changing the initial mesh and the rigidity matrix. Instead, the new degrees of freedom are added as a separate block to the solution. Several issues are not displayed in the literature regarding this method; an important question is the accuracy of satisfying the traction continuity at the edge of the patch.

2. PROBLEM FORMULATION

Consider an elastic body occupying a volume V, containing a crack S (Figure 1a). Displacement and traction boundary conditions are imposed over surfaces ∂V_u and ∂V_T, respectively, where $\partial V_u + \partial V_T = \partial V$. We shall seek the displacements as a superposition of two terms:

$$u_i(x,y,z) = u_i^0(x,y,z) + u_i^c(x,y,z), \tag{1}$$

where $u_i^0(x,y,z)$ are functions continuous through the entire body V, and $u_i^c(x,y,z)$ are functions discontinuous at the surface S. Displacement field (1) is assumed to be kinematically admissible. In addition we define a volume Γ, which includes the crack surface S, which also may be a part of the boundary $\partial\Gamma$. The functions $u_i^c(x,y,z)$ are required to vanish outside and at the boundary of the volume Γ

$$u_i^c(x,y,z) = 0, \{x,y,z \,/\, (x,y,z) \notin \Gamma \text{ and } (x,y,z) \in \partial\Gamma - S\}. \tag{2}$$

It is noted that no assumptions are made by introducing Equations (1) and (2). The stress fields corresponding to the displacement fields $u_i^0(x,y,z)$ and in general will be discontinuous at the boundary $\partial\Gamma$ and

$$\lim_{\beta\to 0} \sigma_{ij}^0(M+\beta\vec{n})n_j = \lim_{\beta\to 0} [\sigma_{ij}^0(M-\beta\vec{n}) + \sigma_{ij}^c(M-\beta\vec{n})]n_j, \quad \beta > 0 \tag{3}$$

where M $\in \partial\Gamma$ and $\vec{n}$ is an outside normal to $\partial\Gamma$. It is of practical interest of how to obtain the class of solutions when $\sigma_{ij}^c(M) = 0$, $M \in \partial\Gamma$. The importance of this requirement can be appreciated by using numerical approximations to obtain the displacement functions in Equation (1). If this requirement is not satisfied, then the stress σ_{ij}^0 will experience a discontinuity at the boundary $\partial\Gamma$ which, if not properly built into displacement approximation $u_i^0(x,y,z)$, will cause oscillatory behavior. Yet the attractiveness of the entire concept of patch superposition lays in the ability to use the same approximation for $u_i^0(x,y,z)$ as for the uncracked body. The following variational equation will be shown to provide the condition $\sigma_{ij}^c(M) = 0$, $M \in \partial\Gamma$:

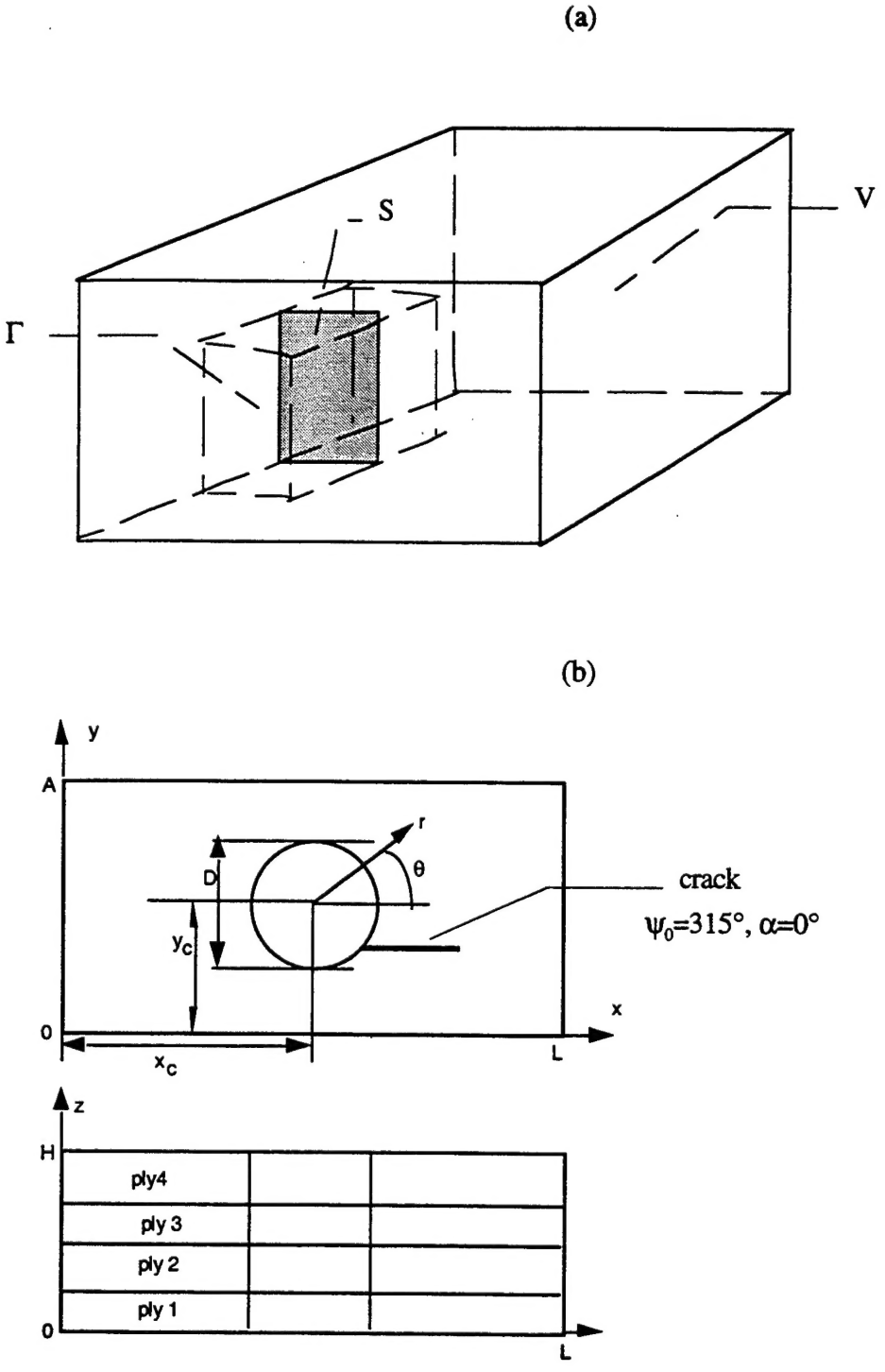

Figure 1. Illustration of Displacement Field Superposition Concept: Multilayered Plate with (a) a Hole and (b) a Crack.

$$\delta\Bigg(-\iiint_{V-\Gamma} U(u^0_{(i,j)})dV-\iiint_{\Gamma} U(u^0_{(i,j)}+u^c_{(i,j)})dV$$
$$+\iint_{\partial\Gamma}\sigma^c_{ij}n_j u^0_i ds \qquad (4)$$
$$\iint_{\partial V_T} T_i^{\partial V}u_i^0 ds+\iint_S [T_i^+(u_i^{c+}+u_i^0)-T_i^-(u_i^{c-}+u_i^0)]ds\Bigg)=0$$

where $u_{(i,j)}=\frac{1}{2}(u_{i,j}+u_{m,i})$, $\sigma_{ij}=Q_{ijkl}u_{(k,l)}$, $U(u_{(i,j)})=\frac{1}{2}Q_{ijkl}u_{(i,j)}u_{(k,l)}$, Q_{ijkl} are the elastic constants, superscripts "c+" and "c-" denote the two crack faces, and $T_i^+$and T_i^- denote the external tractions applied to the latter surfaces. The variation upon $u_i^c(x,y,z)$ yields:

$$\iiint_{V-\Gamma}\sigma^0_{ij,j}\delta u_i^0 dV+\iiint_{\Gamma}(\sigma^0_{ij,j}+\sigma^c_{ij,j})\delta u_u^0 dV+$$
$$+\iint_{\partial\Gamma}\left((\sigma^0_{ij}|_{V-\Gamma}-\sigma^0_{ij}|_{\Gamma}\right)n_j\delta u_i^0 ds+ \qquad (5)$$
$$\iint_{\partial V_T}(\sigma^0_{ij}n_j-T_i^{\partial V})\delta u_u^0 ds+\iint_S(\sigma^{c+}_{ij}-\sigma^{c-}_{ij})n_j-T_i^++T_i^-]\delta u_i^0=0$$

The surface integral upon $\partial\Gamma$ is obtained by taking into account the respective surface integral in (5), where n_i is an outwards relative to volume Γ normal vector. The traction contributions of the stresses, created by the $u_i^0(x,y,z)$ displacement field coming from the first and second volume integral in Equation (4), are distinguished because according to Equation (3), they can be unequal on the boundary $\partial\Gamma$. However due to arbitrary variation, δu_i^0 on the boundary $\partial\Gamma$, we have

$$\left((\sigma^0_{ij}|_{V-\Gamma}(M)-\sigma^0_{ij}|_{\Gamma}(M)\right)n_j=0, M\in\partial\Gamma \qquad (6)$$

The surface integrals upon the crack surface and the external surface ∂V_T are responsible for satisfaction of the applied external traction boundary conditions.

Variation upon $u_i^c(x,y,z)$ provides:

$$-\iiint_{\Gamma}(\sigma_{ij,j}^0+\sigma_{ij,j}^c)\delta u_i^c dV+$$

$$+\iint_{\partial\Gamma}\left(\sigma_{ij}^0|_{\Gamma}+\sigma_{ij}^c\right)n_j\delta u_i^c ds+\iint_{\partial\Gamma}\delta\sigma_{ij}^c n_j u_i^0 ds$$

$$+\iint_{S}\left((\sigma_{ij}^{c+}+\sigma_{ij}^0)n_j-T_i^+\right)\delta u_i^{c+}ds+\iint_{S}\left((\sigma_{ij}^{c-}+\sigma_{ij}^0)n_j-T_i^-\right)\delta u_i^{c-}ds=0$$

Both surface integrals over $\partial\Gamma$ vanish, one due to the boundary condition (2) and the second due to $\sigma_{ij}^c(M)n_j=0, M\in\partial\Gamma$, which follows from Equation (6).

3. COMPOSITE LAMINATE WITH A HOLE CONTAINING MATRIX CRACKS

Consider a rectangular orthotropic plate containing a circular hole having a diameter D as shown in Figure 1b. The plate consists of N plies of total thickness H in the z-direction and has a length L in the x-direction and width A in the y-direction. Uniaxial loading of the plate in the x-direction is considered. At the opposite edges of the plate, x=0,L, constant displacement in the x-direction is prescribed, and other displacement components at these edges are presumed to be zero:

$$\begin{aligned} &u_x(0,y,z) = -u_L,\ u_y(0,y,z) = u_z(0,y,z) = 0 \\ &u_x(L,y,z) = u_L,\ u_y(L,y,z) = u_z(L,y,z) = 0. \end{aligned} \tag{7}$$

A cylindrical coordinate system r,θ,z is introduced at the center of the hole. The θ=0° coincides with the x-axis.

A crack of length l emanating from the hole edge at $\theta=Y_0$ in the s-th ply and propagating in the direction $\theta=\alpha$ is considered. The crack surface S is defined as

$$\begin{aligned} &x = \frac{D}{2}\cos\psi_0 + \xi \cdot l\cos\alpha + x_c,\ 0 \le \xi \le 1, \\ &y = \frac{D}{2}\sin\psi_0 + \xi \cdot l\sin\alpha + y_c,\ 0 \le \xi \le 1, \\ &z^{(s-1)} \le z \le z^{(s)} \end{aligned} \tag{8}$$

where the s-th ply occupies a region $z^{(s-1)} \le z \le z^{(s)}$.

4. SPLINE APPROXIMATION OF DISPLACEMENTS

The displacement field $u_i^0(x,y,z)$ is approximated, according to Iarve [5]. Cubic spline functions are used. The displacements are continuous through the laminate; the strains and stresses are continuous within a homogeneous ply. Curvilinear transformation, which maps the x,y plane of the plate with a hole into a region $0\le\rho\le1$, $0\le\phi\le2\pi$, was defined as follows:

$$\begin{aligned} x &= \frac{D}{2}F_1(\rho)\cos\phi + L\cdot F_2(\rho)\alpha(\phi) + x_c \\ y &= \frac{D}{2}F_1(\rho)\sin\phi + A\cdot F_2(\rho)\beta(\phi) + y_c \end{aligned}, \tag{9}$$

where

$$F_1(\rho) = \begin{cases} 1+\kappa\cdot\rho, \rho \le \rho_h \\ \dfrac{(1+\kappa\cdot\rho_h)(1-\rho)}{1-\rho_h}, \ \rho_h \le \rho \le 1 \end{cases} \qquad F_2(\rho) = \begin{cases} 0, \rho \le \rho_h \\ \dfrac{\rho-\rho_h}{1-\rho_h}, \ \rho_h \le \rho \le 1 \end{cases}$$

The coordinate line ρ=0 describes the contour of the hole, and the coordinate line ρ=1 describes the rectangular contour of the plate. Inside the near-hole region, $D/2\le\rho\le(1+\kappa)D/2$, which corresponds to $0\le\rho\le\rho_h$, a simple relationship between the cylindrical coordinates and the curvilinear coordinates ρ,ϕ exists: $\rho-\frac{D}{2}=\frac{D\kappa}{2}\rho$ and $\theta=\phi$. The width of this region will be chosen three-hole radii, i.e., $\kappa\rho_h$=3. Beyond this region a transition between the circular contour of the opening and the rectangular contour of the plate occurs. Functions $\alpha(\phi)$ and $\beta(\phi)$ were defined [5], so that the parametric equations $x=\alpha(\phi)+x_c$, $y=\beta(\phi)+y_c$ describe the rectangular contour of the plate, where $0\le\phi\le\phi^{(1)}$ corresponds to $0<x\le L$, $y=A$, $\phi^{(1)}\le\phi<\phi^{(2)}$ corresponds to $x=0$, $0<y\le A$, $\phi^{(2)}\le\phi\le\phi^{(3)}$ corresponds to $0\le x<L$ and $y=A$ and $\phi^{(3)}\le\phi<2\pi$ corresponds to $x=L$, $0\le y<A$.

Displacement components in the x, y and z coordinate directions were approximated by using cubic polynomial spline function of generalized curvilinear coordinates ρ, ϕ, and z as follows:

$$\begin{aligned} u_x &= \mathbf{C}_1^{(s)}\vec{\chi}^{(s)}\mathbf{U}_s^* - \vec{\chi}^{(s)}\mathbf{E}_0^*\cdot u_L + \vec{\chi}^{(s)}\mathbf{E}_L^*\cdot u_L, \\ u_y &= \mathbf{C}_2^{(s)}\vec{\chi}^{(s)}\mathbf{V}_s^*, \\ u_z &= \mathbf{C}_3^{(s)}\vec{\chi}^{(s)}\mathbf{W}_s^*. \end{aligned} \tag{10}$$

where unknown vectors $\mathbf{U}_s$, $\mathbf{V}_s$, $\mathbf{W}_s$ contain unknown displacement spline approximation coefficients. Bold type here and below will be used to designate matrices and vectors, and the superscript star means the transpose operation. The vector of the three-dimensional spline approximation functions was defined as:

$$\left\{\vec{\chi}^{(s)}\right\}_q = R_i(\rho)\Phi_j(\phi)Z_l^{(s)}(z),$$
$$q = l+(j-1)(n_s+3)+(i-1)(n_s+3)k, l=1,\ldots,n_s+3, j=1,\ldots,k, i=1,\ldots,m+3. \tag{11}$$

where sets of B-type cubic basis spline functions $\left\{R_i(\rho)\right\}_{i=1}^{m+3}$, $\left\{\Phi_i(\phi)\right\}_{i=1}^{k+3}$, $\left\{Z^{(s)}i(z)\right\}_{i=1}^{n_s+3}$ along each coordinate were built upon subdivisions: $0=\rho_0<\rho_1<\ldots<\rho_m=1$, $0=\phi_0<\phi_1<\ldots<\phi_k=2\pi$, $z^{(s-1)}=z_0<z_1<\ldots<z_{n_s}=z^{(s)}$ so that the s-th ply occupies a region $z^{(s-1)}\le z\le z^{(s)}$, and n_s is the number of sublayers in each ply. The subdivision of the ρ coordinate is essentially nonuniform. The interval size increases in geometric progression beginning at the hole edge. The region $0\le\rho\le\rho_h$ in which the curvilinear transformation is quasi-cylindrical, is subdivided into m_0 intervals, so that $\rho_h=\rho_{m_0}$. Numbers of intervals of subdivision m, k, n_s in each direction, along with the mesh nonuniformity characteristics such as m_0 and the consecutive interval ratio, determine the accuracy of the solution and the size of the problem. Nonsquare boundary matrices $\mathbf{C}_1^{(s)}$,$\mathbf{C}_2^{(s)}$,$\mathbf{C}_3^{(s)}$ and constant vectors $\mathbf{E}_0$,$\mathbf{E}_L$ are defined, so that the approximation (10) provides a kinematically admissible displacement field for any coefficients $\mathbf{U}_s$,$\mathbf{V}_s$,$\mathbf{W}_s$, i.e., satisfying boundary conditions (7). The components of vectors $\mathbf{E}_0$,$\mathbf{E}_L$ are equal to 1 if the same components of $\vec{\chi}^{(s)}$ are nonzero at $\rho=1$, $\phi^{(1)}\le\phi<\phi^{(2)}$ ($x=0$, $0<y\le A$) and $\rho=1$, $\phi^{(3)}\le\phi<2\pi$ ($x=L$, $0<y\le A$), respectively. All other components of the vectors $\mathbf{E}_0$,$\mathbf{E}_L$ are equal to zero. The boundary matrices are obtained by deleting a number of rows from the unit matrix. The rows 10 deleted are the ones having a nonzero scalar product with $\mathbf{E}_0$ or $\mathbf{E}_L$.

4.1 Model 1: Spline Approximation of Displacements in the Overlay Patch

The overlay displacement field $u_i^c(x,y,z)$ was also approximated using cubic spline functions. The location of the overlay mesh was defined by equations:

$$x=\frac{D}{2}\cos\psi+\xi\cdot\left(l+\frac{d}{2}(\cos(\psi_0+\alpha)-\cos(\psi-\alpha))\right)\cos\alpha+x_c,$$
$$y=\frac{D}{2}\sin\psi+\xi\cdot\left(l+\frac{d}{2}(\cos(\psi_0+\alpha)-\cos(\psi-\alpha))\right)\sin\alpha+y_c, \tag{12}$$
$$z^{(s-1)}\le z\le z^{(s)}$$

where $0 \le \xi \le 1$, $\psi_0-\Delta_1 \le \psi \le \psi_0+\Delta_2$. The boundary $\xi=0$ coincides with the part of the hole boundary, and the boundary $\xi=1$ is a straight line going through the crack tip. Boundaries $\psi=\psi_0-\Delta_1$, $\psi=\psi_0+\Delta_2$ are parallel to the crack face. Subdivisions are introduced $0=\xi_0<\xi_1<\xi_2<\ldots<\xi_{m_c}=1$, $\psi_0-\Delta_1=\psi_{-k_1}<\psi_{-k_1+1}<\ldots<\psi_0<\psi_1<\ldots<\psi_{k_2}=\psi_0+\Delta_2$. The subdivisions are uniform, and the crack surface $\psi=\psi_0$ is a coordinate line of the ψ subdivision, total number of intervals of the ψ subdivision is $k_c=k_1+k_2$. The coordinate z is subdivided into the same sublayers as the laminate, i.e., $z^{(s-1)}=z_0<z_1<\ldots<z_{n_s}=z^{(s)}$. An example of the initial mesh (9) with m=18, m_0=14, q=1.0, $\kappa\rho_h$=3, k=48, L/A=2, L/D=10, x_c=L/2, y_c=A/2 is given in Figure 2a, an overlay mesh with α=90°, ψ_0=90°, m_c=9, $k_1=k_2$=7, $\Delta_1=\Delta_2$=30°, l=0.1L is shown in Figure 2b and superimposed meshes in Figure 2c. Basic systems of spline functions are built upon the above subdivisions. Two independent sets of splines are built upon ψ:k_1+3 functions on the interval $\psi_0-\Delta_1=\psi_{-k_1}<\psi_{-k_1+1}<\ldots<\psi_0$ and k_2+3 functions on the interval $\psi_0<\psi_1<\ldots<\psi_{k_2}=\psi_0+\Delta_2$. That way no continuity conditions are imposed at $\psi=\psi_0$. Spline approximation of the overlay displacements can be expressed as

$$u_x^c=\mathbf{C}_1^c\vec{\chi}_c\mathbf{U}_c^*,\ u_y^c=\mathbf{C}_2^c\vec{\chi}_c\mathbf{V}_c^*,\ u_z^c=\mathbf{C}_3^c\vec{\chi}_c\mathbf{W}_c^*. \tag{13}$$

$$\{\vec{\chi}_c\}_q=R_i^c(\xi)\Phi_j^c(\psi)Z_l^s(z),$$
$$q=l+(j-1)(n_s+3)+(i-1)(n_s+3)[k_c+6],\ l=1,\ldots,n_s+3, j=1,\ldots,k_c+6, i=1,\ldots,m_c+3.$$

Vectors $\mathbf{U}_c,\mathbf{V}_c,\mathbf{W}_c$ contain the unknown spline approximation coefficients. Sets of basic spline functions are denoted as $\{R_i^c(\xi)\}_{i=1}^{\cdot}$, $\{\Phi_i^c(\psi)\}_{i=1}^{\cdot}$, $\{Z_i^s(z)\}_{i=1}^{\cdot}$, the z-functions are the same as in (10). To provide the boundary conditions (2), the boundary matrices have to be defined, so that all components of the spline function vector different from zero at $\psi=\psi_0-\Delta_1$, $\psi=\psi_0+\Delta_2$, $\xi=1$ and $z=z^{(s-1)}$, $z=z^{(s)}$ will not contribute to displacement values. According to boundary properties of spline functions given by Iarve [5], the only components of the spline function vector contributing at these surfaces are the ones containing functions $\Phi_j^c(\psi)$, j = 1, k_c+6; $R_i^c(\xi)$, $i=m_c+3$ and $Z_l^s(z)$, $l=1, n_s+3$. The boundary matrices are obtained from unit matrices by deleting the rows having a nonzero scalar product with $\mathbf{E}^c$, where a component of $\mathbf{E}^c$ is equal to unity if the corresponding component of the vector $\vec{\chi}_c$ contains the aforementioned functions and zero otherwise.

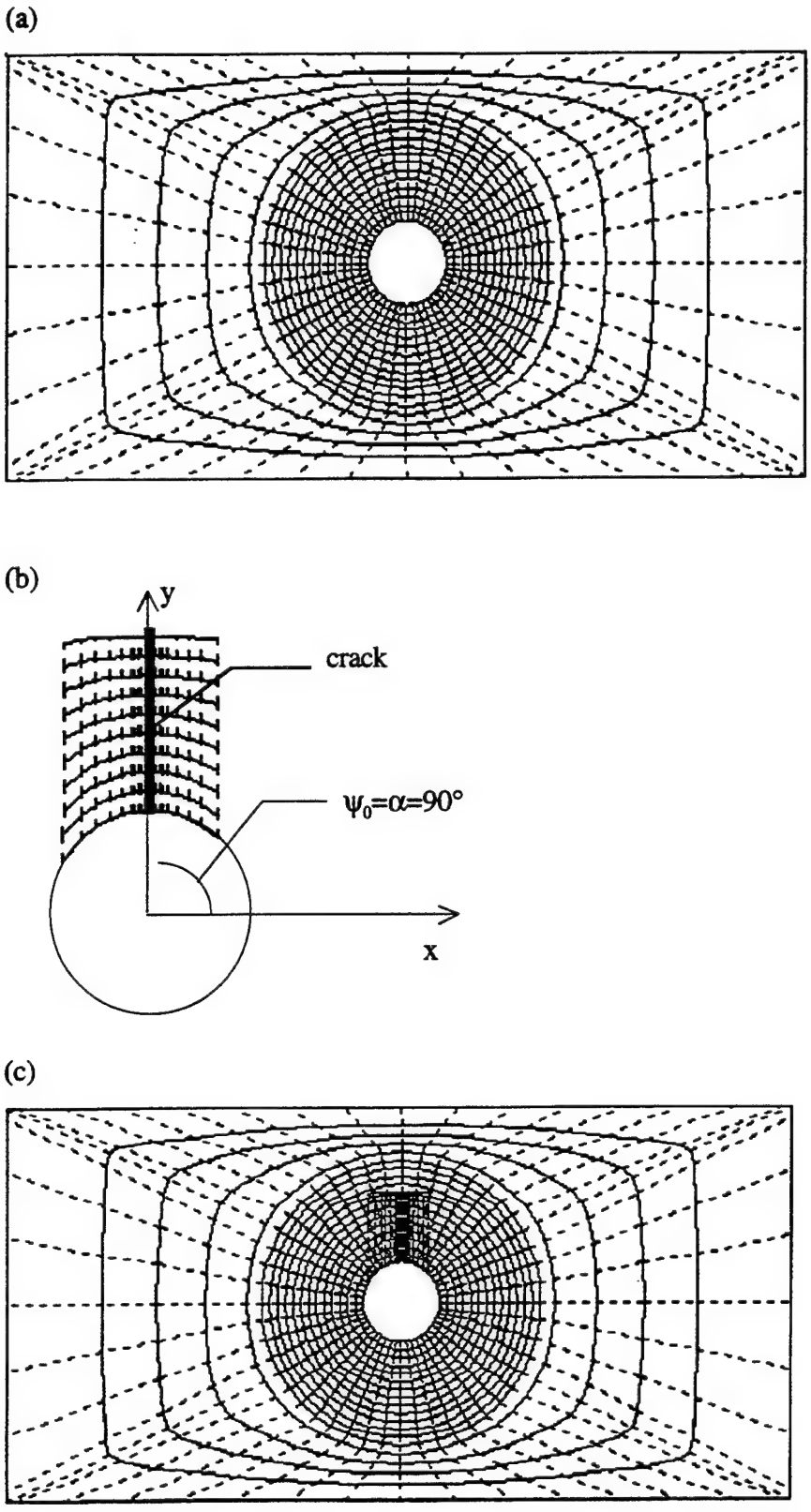

Figure 2. (a) Original Mesh, (b) Overlay Mesh, and (c) the Superposition.

4.2 Model 2: Spline Basis Decomposition Method

An alternative approach, which circumvents the compatibility conditions resolved by functional (4), is to create a complete system of basic functions in the spline function space, which provides displacement discontinuity along the crack surface S described by Equation (8). It is possible to build such a basis without modifying the spline functions of approximation (10) but rather by adding locally new splines to describe the discontinuity of displacements. The idea will be illustrated on a one-dimensional example. Consider an interval subdivided into seven subintervals (Figure 3). We shall build the spline approximation of a function f(x), which is discontinuous at the point $x=x_4$, and continuously differentiable elsewhere on the interval $[x_0,x_7]$. A straightforward solution lies in using two sets of spline basis functions built over intervals $[x_0,x_4]$ and $[x_4,x_7]$, respectively. The total number of spline functions will be m+6, where m is the number of intervals (m=7). In this case, however, most of the splines of such a basis do not coincide with the spline functions of continuously differentiable approximation on the entire interval $[x_0,x_7]$ as shown in Figure 3a. These functions are denoted $\{X_{3,i}(x)\}_{i=1,m+3}$, so that a function $\bar{f}$

$$\bar{f}(x) = \sum_{i=1}^{m+3} f_i X_{3,i}(x)$$

is continuously differentiable at each point between x_0 and x_7. New spline functions $X'_{3,i}(x)$ are formed by partitioning splines which $X_{3,i}(x_4)>0$. These new splines are defined as follows

$$X'_{3,i}(x) = \begin{cases} X_{3,i}(x), x \geq x_4 \\ 0, x < x_4 \end{cases}$$

In the present example there are three new splines created i=5,6,7 as shown in Figure 3b. A function f(x)

$$f(x) = \sum_{i=1}^{m+3} f_i X_{3,i}(x) + \sum_{i=5}^{7} f'_i X'_{3,i}(x) \qquad (14)$$

is discontinuous at $x=x_4$ and continuously differentiable at all other points of the interval. It can also be shown that functions $\{X_{3,i}(x)\}_{i=1,m+3}$ and $\{X'_{3,i}(x)\}_{i=5,7}$ form a complete set of basis functions. Thus we have built a complete set of basis functions by adding several new splines to the initial continuous approximation spline functions.

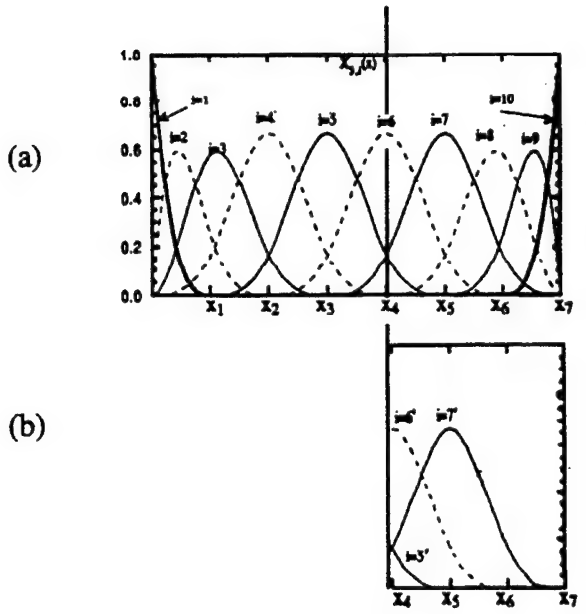

Figure 3. Spline Basis Decomposition Method on a One-Dimensional Example: (a) Original, Continuously Differentiable Basis Functions and (b) Additional Spline Functions.

In the case of a crack emanating from the hole edge, we need to build essentially a two-dimensional set of splines analogous to the $X'_{3,i}(x)$ in Equation (14). In the z-direction the same spline functions as in the previous section will be used. A parametric representation ξ,τ of the x,y plane is defined:

$$\begin{aligned} x &= \frac{D}{2}\cos\psi_0 + \xi \cdot l\cos\alpha - \tau\sin\alpha + x_c, \xi > 0 \\ y &= \frac{D}{2}\sin\psi_0 + \xi \cdot l\sin\alpha - \tau\cos\alpha + y_c, \xi > 0 \end{aligned} \tag{15}$$

The spline functions in Equation (11) are examined, and those nonzero at the crack line $\tau=0$ are partitioned to create new spline functions

$$\left\{\vec{X}_c^{'}\right\}_q = R_i^{'}(\rho)\Phi_j^{'}(\phi)Z_i^{(s)}(z), \tag{16}$$

$$R_i^{'}(\rho)\Phi_j^{'}(\phi)Z_l^{(s)}(z) = \begin{cases} R_i(\rho)\Phi_j(\phi)Z_l^{(s)}(z), \tau \geq 0 \\ 0, \tau < 0 \end{cases}$$

Additional or superimposed spline approximations can be written similar to Equation (13):

$$u_x^c = \mathbf{C}_1^c \vec{\chi}_c^{'} \mathbf{U}_c^*, u_y^c = \mathbf{C}_2^c \vec{\chi}_c^{'} \mathbf{V}_c^*, u_z^c = \mathbf{C}_3^c \vec{\chi}_c^{'} \mathbf{W}_c^*. \tag{17}$$

where the vector of spline functions is defined similar to (11), but only the spline functions (16) are used. Variational formulation in this case is straightforward, since no incompatibility exists between shape functions (11) and (17). The variational equation will be simplified as:

$$\delta\left(-\iiint_V U(u^0_{(i,j)} + u^0_{(i,j)} + u^c_{(i,j)})dV \right.$$
$$\left. \iint_{\partial V} T_i^{\partial V} u_i^0 ds + \iint_S [T_i^+(u_i^{c+} + u_i^0) - T_i^-(u_i^{c-} + u_i^0)] \right) \tag{18}$$

5. NUMERICAL RESULTS

A unidirectional AS4/3501-6 laminate [90_2] was considered first. The mechanical properties were E_1 = 138 GPa, $E_2 = E_3$ = 10.3 GPa, $\nu_{13} = \nu_{12}$ = 0.3, ν_{23} = 0.55, $G_{12} = G_{13}$ = 5.52 GPa and G_{23} = 3.45 GPa. The geometric dimensions were L = 6.35 cm, A = L/2, and the diameter of a central hole was D = L/10. A crack l = 0.1 L was considered emanating from the hole edge at $\theta = 90°$ ($\psi_0 = 90°$) in the $\alpha = 90°$ direction. The ρ,ϕ subdivision with m = 18, m_0 = 14, q = 1.0, $\kappa\rho_h$ = 3, and k = 48, shown in Figure 2a, along with two sublayers in the z-direction, were utilized to approximate the $u_i^0(x,y,z)$ displacement field.

Model 1 was used to approximate the overlay displacements. The overlay mesh was imposed only on one side of the crack, so that $\Delta_1 = 30°$ and $\Delta_2 = 0$, with 10 ψ-intervals between ψ_0-Δ_1 and ψ_0. Ten uniform ξ intervals were used. Stress distribution in the cross section $\theta = 90°$ as a function of distance from the hole edge is examined in Figure 4a. The σ_{xx} stress component in the plate without a crack is shown for comparison by a thick dashed line. The stress results are normalized to the average far-field stress in an uncracked laminate in the x-direction , calculated as

$$\sigma_0 = \int_0^H \int_0^A \sigma_{xx}(L,y,z)dydz.$$

The results for the cracked laminate are obtained using the variational equation (4), neglecting the surface integral upon the boundary $\partial\Gamma$. Stress distribution in the cracked laminate is shown by the solid and thin dashed lines. In addition the crack opening displacement is also shown, normalized to the applied displacement u_L [Equation (7)]. Along the crack surface in the vicinity of the crack tip σ_{xx}, stress exhibits oscillatory behavior. However the true effect of the incompatibility of the overlay and underlying meshes is clearly illustrated in Figure 4b, where the stresses along the boundary of the patch region $\psi = \psi_0$-Δ_1 are shown. The thin dashed line shows the stress designated in (5) as $\sigma_{xx}^0|_{V-\Gamma}(M)$, and the solid line stress $\sigma_{xx}^0|_{\Gamma}(M) + \sigma_{xx}^c(M)$, where $M \in \partial\Gamma$. A significant stress discontinuity is obvious. The solid dashed line shows the σ_{xx} stress in a cross section symmetric to $\psi = \psi_0$-Δ_1 against the plane $\theta = 90°$. Ideally, all three curves shown in Figure 4b have to coincide.

Model 2 will be used to approximate the overlay displacements in the same problem. The displacements $u_i^0(x,y,z)$ are the same as before. The superimposed shape functions are formed according to rule (16) and no additional mesh is required. Variational Equation (18) is used. Figure 5a shows the σ_{xx} stress distribution in the cross section $\theta = 90°$. The thick dashed line

(a)

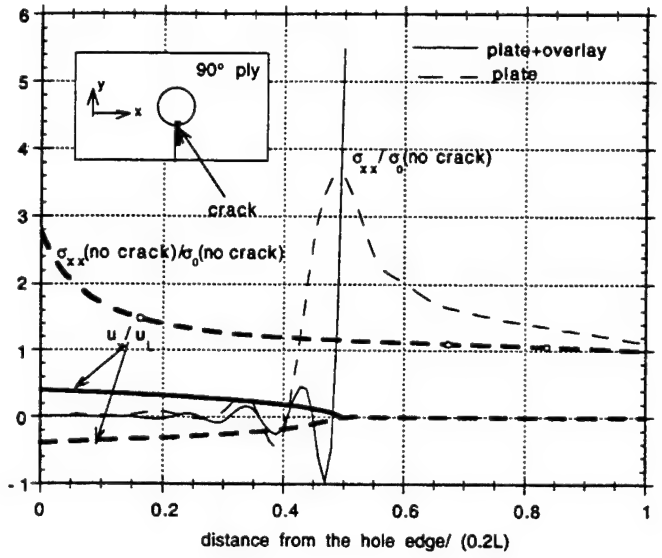

(b)

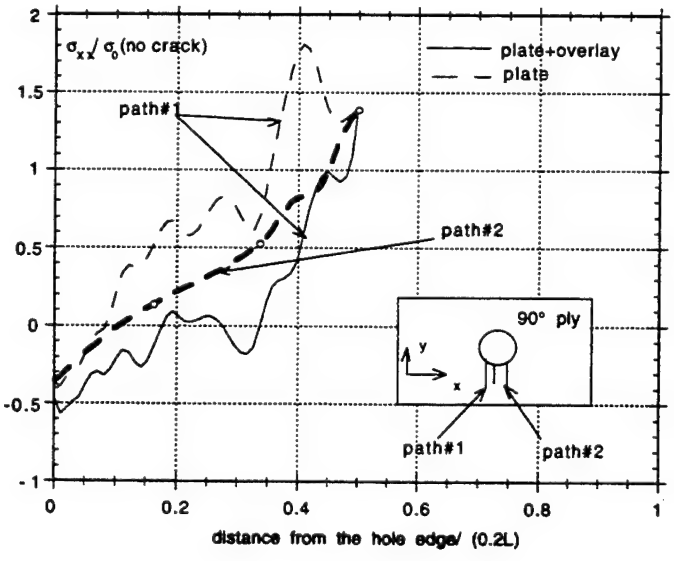

Figure 4. Mesh Overlay Model 1, σ_{xx} at (a) $\theta = 90°$ and (b) Overlay Mesh Boundary.

(a)

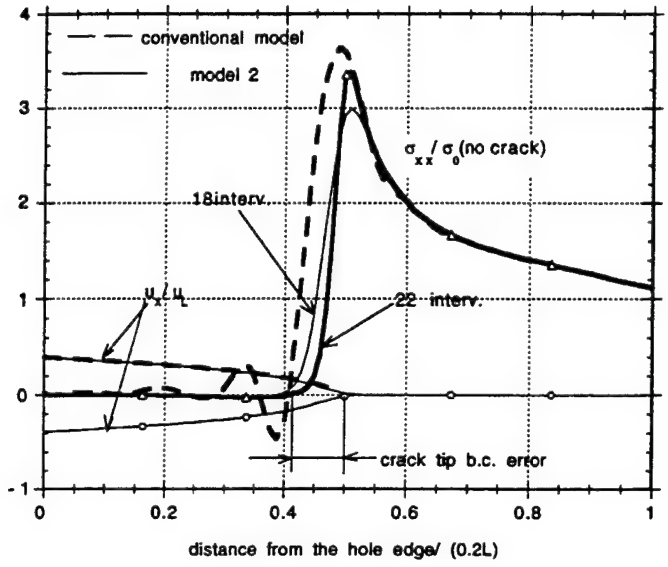

(b)

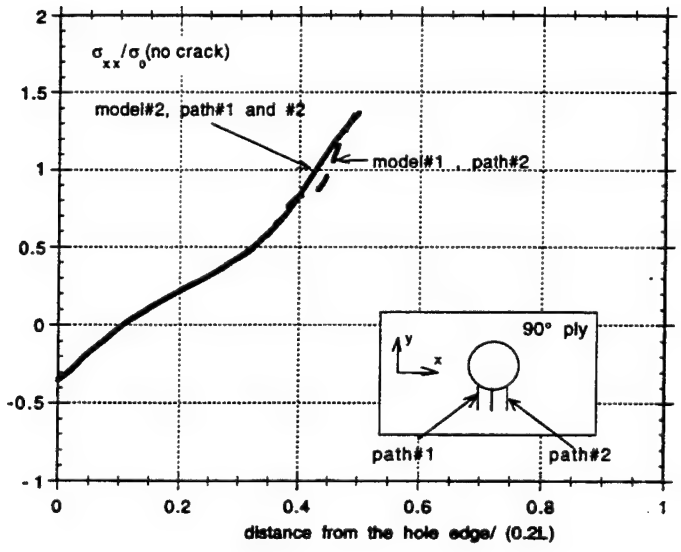

Figure 5. Mesh Overlay Model 2, at (a) $\theta = 90°$ and (b) σ_{xx} at Model 1 Overlay Mesh Boundary.

was copied from Figure 4a. The stress calculated by using Model 2 for overlay displacement approximation is shown by a thin solid line. No oscillations of the σ_{xx} stress along the crack face is present. There is a region in the vicinity of the crack tip marked as a crack tip boundary condition error. In this region both the crack opening displacement and the stress normal to the crack faces are nonzero. By increasing the density of the subdivision by splitting four intervals near the crack tip, this region reduces. The result for the increased subdivision is shown by a thick solid line. The stresses at the same cross sections, as shown in Figure 4b, are displayed in Figure 5b. The stress obtained by using Model 2 along the cross section $\psi = \psi_0 - \Delta_1$, and the one symmetric against the plane $\theta = 90°$, are indistinguishably close-solid lines. The dashed line has been copied from Figure 4b and shows overall agreement with the Model 2 results, except a kink near the end of the pitch which is likely the result of untreated compatibility of the meshes in Model 1. Figure 6 shows the hoop and the radial stress in uncracked and cracked laminates obtained using Model 2. The displacement field in the uncracked laminate was approximated according to (11) only. Stress is plotted versus the θ angle at the midsurface. The presence of the crack at $\theta = 90°$ increases the hoop stress at $\theta = 270°$. An important observation is that the accuracy of satisfaction of the traction-free boundary condition at the hole edge does not deteriorate while enriching the spline approximation basis with functions (16). Indeed, the σ_{rr} stress distribution for uncracked and cracked laminates is practically the same.

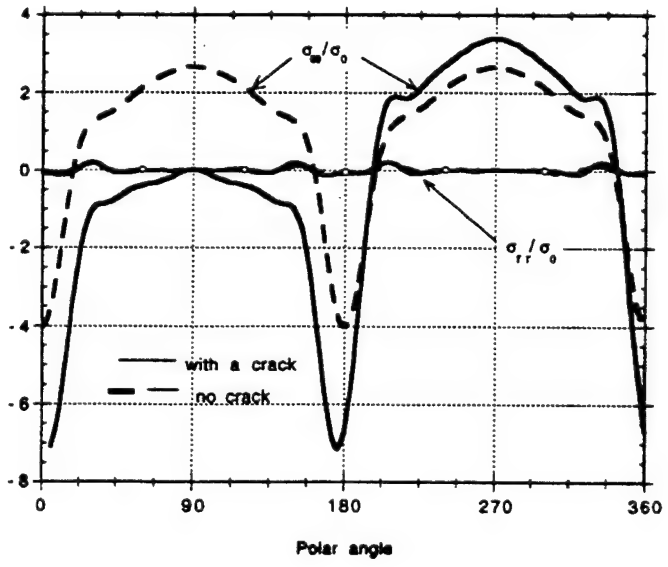

Figure 6. Radial and Hoop Stresses at the Midsurface Around the Circumference of the Hole of the Uncracked and Cracked Laminate.

A $[0_2]$ laminate is considered next. A matrix crack, tangential to the hole edge, is modeled as two cracks of length $l = 0.1$ L emanating at $\theta = 90°$ ($\psi_0 = 90°$) in $\alpha = 0°$ and $\alpha = 180°$ directions. All of the following results are obtained with Model 2 overlay displacement approximation. The applied displacement was $u_L = u_0 = 6.95 \times 10^{-6}$ m. Contour plot of the u_y in units of meters is shown in Figure 7b inside the region designated in Figure 7a. The u_y is positive above the crack and negative below it, reflecting the fact that this crack is open. The normal σ_{yy} and shear σ_{xy} stresses are shown in Figure 7c and 7d. The presence of the crack relieves both stresses in the area above the crack with only stress concentrations at the crack tips.

Finally, a $[0/90]_S$ laminate is considered. The same geometric dimensions as before are used. Each ply is subdivided into two sublayers. Two matrix cracks $\psi_0 = 90°$ and $\psi_0 = 270°$ are considered in the 90° ply, as shown in Figure 8a. The σ_{xx} stress around the hole edge is examined at different through-the-thickness locations. Figure 8b displays the stresses at the midsurface and the 0/90 interface in the 90° ply. The dashed lines are used for uncracked laminates, and the solid lines for cracked laminates. At $\theta = 90°$ and 270° locations at the midsurface, σ_{xx} vanishes at the crack surface. This stress redistribution is very local, and at approximately ±15° away from the crack locations, the stress is equal to that in the uncracked laminate. At the ply interface the crack produces higher stresses because it is impending the interface. In the 0° ply the stresses at $\theta = 90°$ and 270° are slightly higher in the cracked laminate than the uncracked one. It is expected due to the loss of load carrying capacity in the 90° ply.

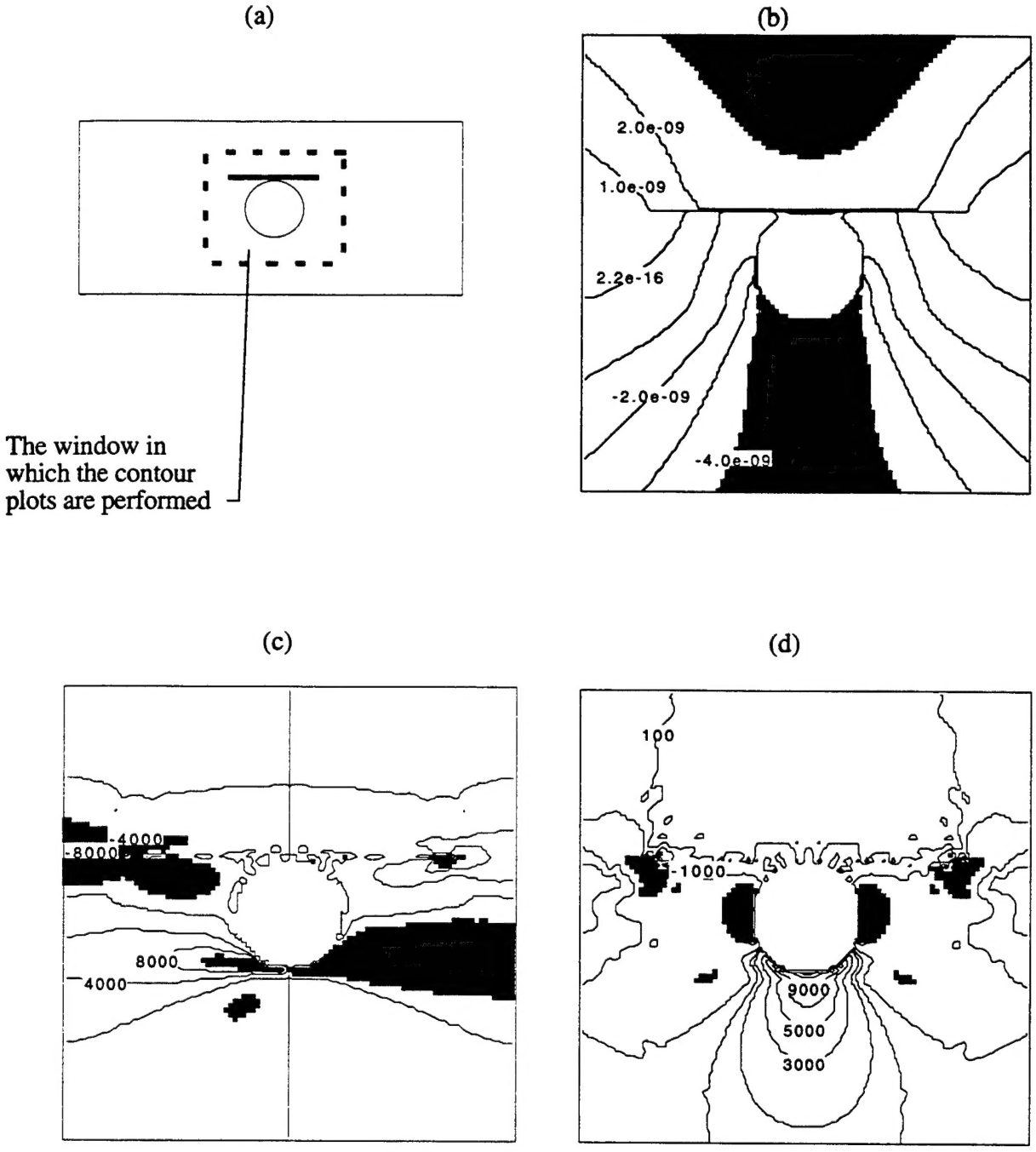

Figure 7. [0_2] Laminate with a (a) Matrix Crack, (b) u_y Displacement, (c) σ_{yy}, and (d) σ_{xy}.

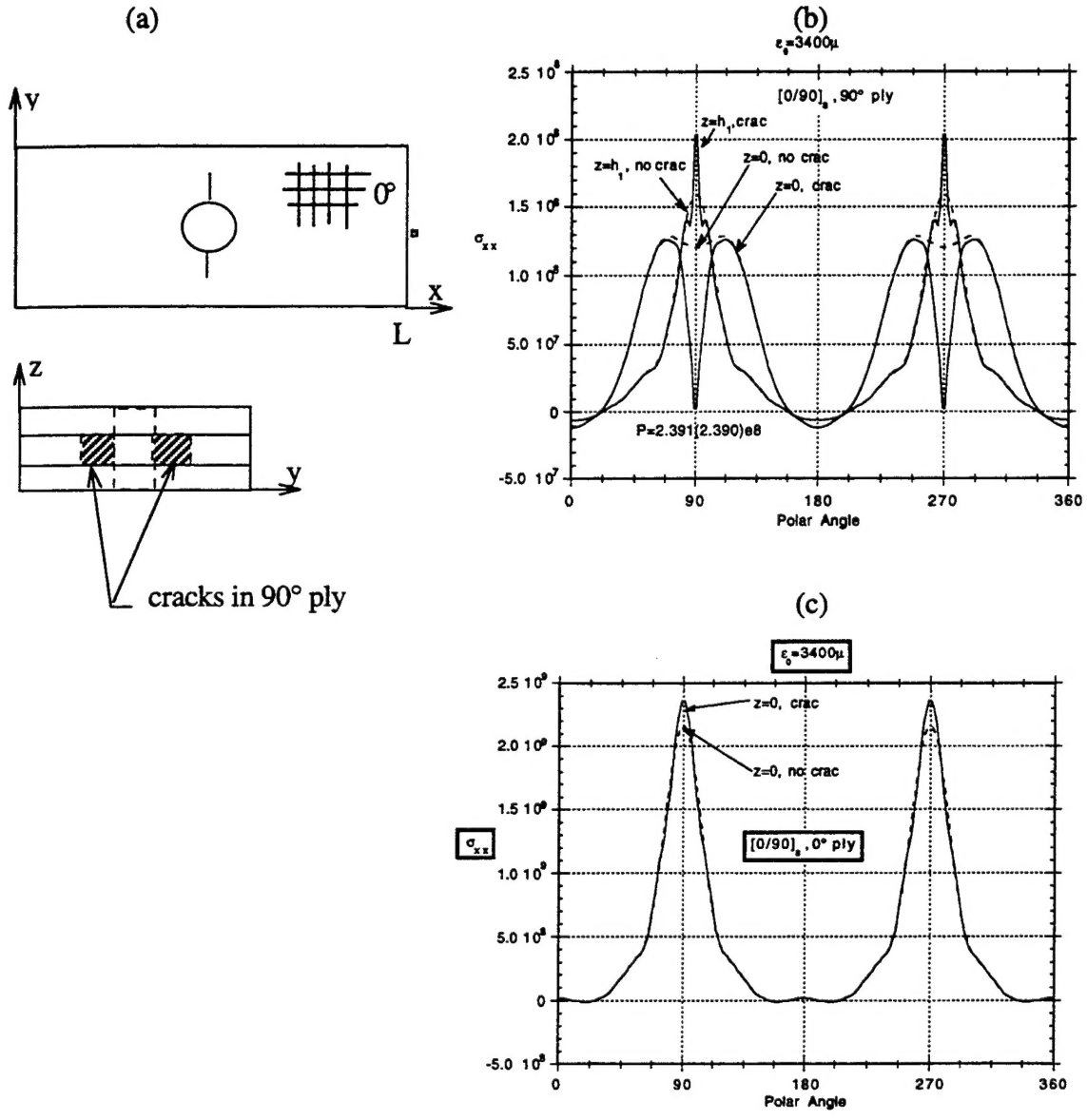

Figure 8. Crack Location and the (a) Coordinate Systems; Hoop Stress Redistribution in the (b) 90° Ply and (c) 0° Ply due to Matrix Cracking. Solid lines = cracked specimen; dashed lines = uncracked specimen.

6. PUBLICATIONS AND PRESENTATIONS

The following publications and presentations were generated during this contractual period:

Iarve, E. V., & Jeffrey R. Schaff. (1996, September). *Stress Analysis of Open and Fastener Hole Composites Based on Three-Dimensional Spline Variational Technique*. Paper presented at AGARD 83 SMP Meeting, Florence, Italy.

Iarve, E. V. (1995). Three-Dimensional Stress Analysis of Fastener Hole Composites. *Proceedings of the ASME Materials Division* (MD-Vol. 69-1, 1995 IMECE).

Iarve, E. V. (1996). Spline Variational Three-Dimensional Stress Analysis of Laminated Composite Plates with Open Holes. *Int. J. of Solids & Structures 33*(14) (pp. 2095-2118).
Iarve, E. V. (1996, September). *3-D Stress Analysis of Composite Laminates with Matrix Cracks Using SVELT*. 1996 SVELT Workshop, WPAFB, OH.

7. REFERENCES

1. Mote, C. D. (1971). Global-Local Finite Element. *Int. J. Numer. Meth. Engng. 3* (pp. 565-574).

2. Raju, I. S. (1986, July). *Multigrid Methods in Structural Mechanics* (NASA Report) (60 pp).

3. Reddy, N. J. (1993). An Evaluation of Equivalent-Single-Layer and Layerwise Theories of Composite Laminates. *Composite Structures 25* (pp. 21-35).

4. Fish, J. (1992). The s-Version of the Finite Element Method. *Composite Structures 43* (pp. 539-547).

5. Iarve, E. V. (1996). Spline Variational Three-Dimensional Stress Analysis of Laminate Composite Plates with Open Holes. *Int. J. Solids & Structures 33*(14) (pp. 2095-2118).